Landslides Triggered by the 2002 Denali Fault, Alaska, Earthquake and the Inferred Nature of the Strong Shaking

Randall W. Jibson,[a] Edwin L. Harp,[a] William Schulz,[a] and David K. Keefer[b]

The 2002 M7.9 Denali fault, Alaska, earthquake triggered thousands of landslides, primarily rock falls and rock slides, that ranged in volume from rock falls of a few cubic meters to rock avalanches having volumes as great as 15×10^6 m^3. The pattern of landsliding was unusual; the number of slides was less than expected for an earthquake of this magnitude, and the landslides were concentrated in a narrow zone 30-km wide that straddled the fault rupture over its entire 300-km length. The large rock avalanches all clustered along the western third of the rupture zone where acceleration levels and ground-shaking frequencies are thought to have been the highest. Inferences about near-field strong shaking characteristics drawn from the interpretation of the landslide distribution are consistent with results of recent inversion modeling that indicate high-frequency energy generation was greatest in the western part of the fault rupture zone and decreased markedly to the east. [DOI: 10.1193/1.1778173]

INTRODUCTION

South-central Alaska and the Alaska Range were severely shaken on the morning of 3 November 2002 by a M7.9* earthquake. The quake triggered 40 km of rupture along the Susitna Glacier fault and 288–296 km of surface rupture along the Denali and Totschunda faults (Figure 1). Seismic shaking triggered numerous landslides and caused liquefaction failures within the central part of the Alaska Range and the surrounding region (Eberhart-Phillips et al. 2003, Harp et al. 2003). Landslides triggered by the earthquake were mainly rock falls and rock slides (in the landslide terminology of Varnes 1978) containing mixtures of fractured rock, soil, ice, and snow. The most spectacular landslides were large rock avalanches having volumes of several million cubic meters that were deposited on the Black Rapids, McGinnis, and West Fork Glaciers.

Quantifying the near-field strong-motion characteristics for this earthquake has been difficult because only one strong-motion accelerograph was present in the near field. The analysis of the pattern of triggered landslides and liquefaction effects may provide some of the best evidence of the characteristics of the strong shaking.

[a] U.S. Geological Survey, Box 25046, MS 966, Denver Federal Center, Denver, CO 80225
[b] U.S. Geological Survey, MS 977, 345 Middlefield Rd., Menlo Park, CA 94025

* All magnitudes in this paper, unless otherwise indicated, are moment magnitudes, **M**.

Earthquake Spectra, Volume 20, No. 3, pages 669–691, August 2004; © 2004, Earthquake Engineering Research Institute

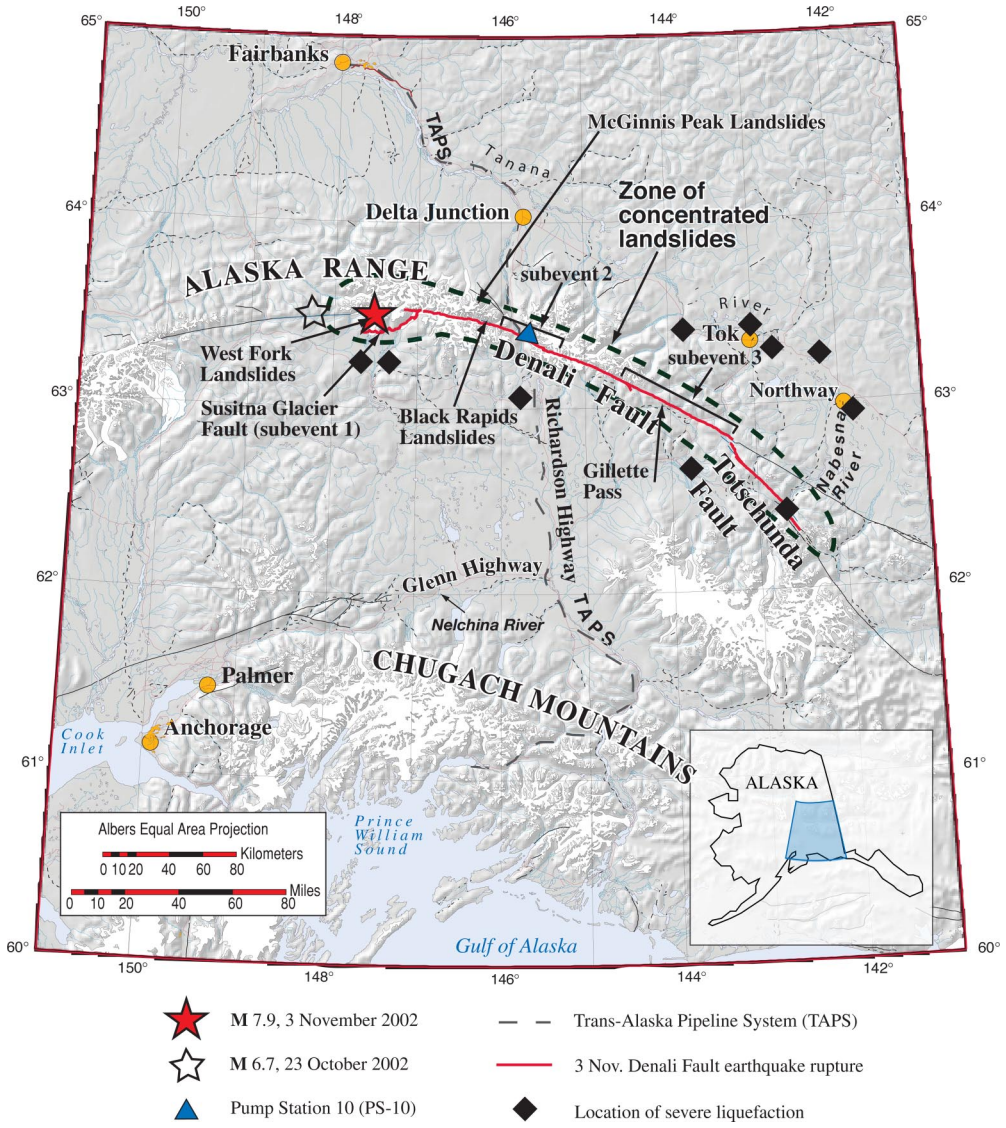

Figure 1. Map showing area of Denali fault earthquake. Area enclosed by heavy dashed line shows zone of concentrated landslides triggered by the earthquake. Earthquake subevent locations from Frankel (2004); liquefaction locations from Kayen et al. (2004, this issue).

Previously published papers discussing these landslides (Eberhart-Phillips et al. 2003; Harp et al. 2003) contain estimates of volumes and distances that were based on initial reconnaissance observations. This paper has updated many of these estimates based on additional fieldwork and analysis; values in this paper supersede those published earlier.

In this paper, we briefly describe the faulting and seismological properties associated with the earthquake, characterize the regional distribution of landslides, describe the largest landslides triggered, and interpret the triggered landslides in terms of inferences on the distribution and characteristics of strong motion associated with this earthquake.

THE DENALI FAULT EARTHQUAKE

The M7.9 earthquake, one of the largest earthquakes in U.S. history, resulted from thrusting along the Susitna Glacier fault and right-lateral movement on the Denali-Totschunda fault system (Figure 1). The Denali fault is one of the longest strike-slip fault systems in the world; it consists of numerous strands along its 2000-km length and is comparable in length to the San Andreas fault that produced the 1906 M7.9 San Francisco earthquake (Miller et al. 2002). The Totschunda fault, a major splay of the Denali fault system, extends for 200 km from its junction with the Denali fault at Mentasta Pass southeast to the Alaska-Yukon Territory border (Plafker et al. 1994, 1977). The Denali and Totschunda faults both show evidence of recent movement. The Susitna Glacier fault was previously unrecognized.

The M7.9 mainshock was preceded by a M6.7 foreshock on 23 October 2002 on the Denali fault (Figure 1). The epicenter of the mainshock was about 22–25 km east of the foreshock. The mainshock consisted of multiple subevents—distinct rupture events within the overall earthquake rupture sequence (Kikuchi and Yamanaka 2002, Choy and Boatwright 2004, Frankel 2004). The first subevent was a M7.2 thrust event on the Susitna Glacier fault. This triggered a second subevent, a right-lateral rupture on the Denali fault centered near the Richardson Highway and the trans-Alaska pipeline. During a third subevent, right-lateral rupture propagated eastward along the Denali fault for 225 km (Frankel et al. 2002) and continued for about 50 km southeastward on the Totschunda fault. Right-lateral slip averaged about 3.5 m and ranged up to almost 9 m. A maximum of about 3 m of vertical movement occurred as both thrust and normal slip. Pre-existing, degraded fault scarps (Plafker et al. 1977) ruptured again at many places during the M7.9 event.

Only one strong-motion accelerograph was operating in the near-field area of the earthquake. Located at Pump Station 10 along the trans-Alaska pipeline (Figure 1), this instrument recorded a peak ground acceleration (PGA) of 0.36 g. Other accelerometers recorded the earthquake at several locations, including Anchorage, Fairbanks, and Valdez. These more distant recordings permitted identification of subevents but were too distant to provide any information on near-field ground accelerations.

DISTRIBUTION AND TYPES OF TRIGGERED LANDSLIDES

The earthquake triggered thousands of landslides from the steep slopes of the Alaska Range. The distribution of landslides was mapped by aerial reconnaissance. The landslides ranged in size from rock falls of a few cubic meters to rock avalanches of several million cubic meters that were triggered on steep rock slopes bordering large valley glaciers. The majority of landslides were shallow rock falls and rock slides from steep slopes. Most slopes in the epicentral area have exposures of weathered bedrock or thin colluvium; landslides generally involved failure of the uppermost few decimeters to

Figure 2. Scattered rock falls (examples shown by arrows) on slopes near the Denali fault. The concentration and size of such rock falls were relatively low for a M7.9 earthquake.

meters of this material, which cascaded down the steep slopes (Figure 2). At the time of the earthquake, most slopes were covered by a thin blanket of snow, and so recent landslides were easily identifiable against the white background of snow.

One unusual aspect of the landslides triggered by this earthquake was their narrow concentration along the fault rupture. Normally, an earthquake of this magnitude would be expected to trigger landslides over a broad region extending perhaps 350 km from the fault and covering an area of 28,000 to perhaps 90,000 km^2 (Keefer 1984 and 2002). In this earthquake, the majority of landslides were concentrated in a narrow band about 30-km wide that straddled the fault rupture for more than 300 km (Figure 1). The largest landslides (described in the following section) clustered at the western part of the fault zone between subevents 1 and 2 (Figure 1), and landslide concentration decreased eastward along the fault zone. We saw only a few scattered landslides at greater distances than 15 km from the fault, on both sides, despite the fact that steep, highly susceptible slopes are abundant well beyond this observed 15-km limit. The most distant triggered landslide we observed was a single rock fall in the Chugach Mountains near Palmer, Alaska, about 250 km southwest of the fault. We also saw several failures in sensitive clay along terraces of the Nelchina River about 150 km from the fault. Other than these, we saw none at distances greater than about 15 km from the fault zone.

Another unusual aspect of the landslides was their relative scarcity. Keefer (2002) examined data from 11 earthquakes for which detailed landslide inventories were compiled and plotted magnitude versus number of landslides triggered. His data suggest that a M7.9 earthquake might be expected to trigger about 80,000 landslides. Although we were unable to compile a detailed inventory, the number of triggered landslides from the

Denali Fault earthquake appeared to be at least an order of magnitude less than this. Likewise, landslide concentrations on the steep slopes near the fault were not as great as we have seen in other recent earthquakes of smaller magnitude, as detailed subsequently in the Discussion section.

LARGE ROCK AVALANCHES

By far the most impressive landslides triggered were several large rock avalanches that spilled onto glaciers in the Alaska Range. Similar avalanches of rock and ice were triggered in the Chugach Range by the 1964 M9.2 Alaska earthquake (Tuthill and Laird 1966, Post 1967). All of the largest rock avalanches triggered by the 2002 M7.9 event were located near the fault ruptures between the first and second subevents. Two of them occurred near subevent 1 on the hanging wall of the Susitna Glacier thrust fault. Another five occurred between subevents 1 and 2 on the flanks of McGinnis Peak and on slopes along the south margin of the Black Rapids Glacier.

MCGINNIS GLACIER LANDSLIDES

The earthquake triggered two huge avalanches of rock and ice from different flanks of McGinnis Peak (see Figure 1). The larger northern failure involved about 15 $\times 10^6$ m^3 of metamorphic rock and glacial ice (about 10 percent ice by volume) that collapsed from the northeast ridge of McGinnis Peak, struck the glacier below the rock face, and then flowed for more than 10 km down the glacier, which has an average surface slope of about 5° (Figure 3).

The source of the landslide is a near-vertical rock face about 800 m high (Figure 4). The source rock is predominantly a dense, greenish-gray, fine-grained metamorphic rock. The source scar is defined by a planar, nearly vertical, slope-parallel joint surface. The surface is stepped, indicating a series of slope-parallel joints spaced a few meters apart. Above the rock scar is a vertical exposure of 15–20 m of glacial ice, which also failed and became part of the avalanche. At the base of the source slope is a deeply scoured bowl-shaped pit where the rock and ice from above struck the glacial surface in free-fall.

The valley walls near the source are nearly vertical and parallel, and they channeled the failed rock and ice directly down the valley on the glacial surface (Figure 5). Snow 50–70 m high on valley walls was covered with dust, indicating that the landslide generated a thick dust plume in front of it (see Figure 4).

About 4 km from the source, landslide debris topped a 150-m-high ridge on the left margin of the glacier. This overtopped feature allows us to estimate the minimum velocity of the rock avalanche by applying an equation proposed by Chow (1959) that is commonly used for such estimates (see, e.g., Evans et al. 2001, Vallance and Scott 1997, Voight and Sousa 1994):

$$v = (2gh)^{0.5} \quad (1)$$

where v is velocity in meters per second, h is runup height in meters, and g is gravitational acceleration (9.81 m/s^2). This equation was developed assuming that gravitational force is the only force resisting flow, and hence the velocity v obtained using equation 1

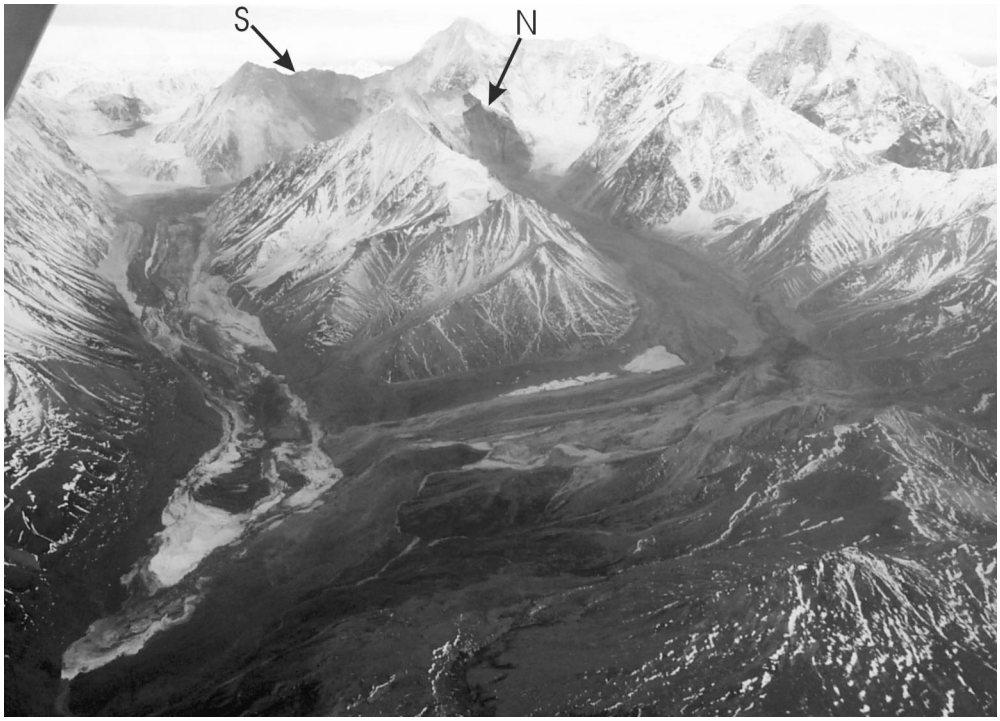

Figure 3. McGinnis Peak rock avalanches (view toward southwest). Two rock avalanches were triggered from the north (N) and south (S) flanks of McGinnis Peak. The rock avalanches both traveled on glacial surfaces and merged in the left center of the photo. The Denali fault lies 9 km to the south.

is the minimum required for a flow to climb to a certain height h until stopped due solely to gravitational forces. Velocity estimates would certainly be greater if other forces resisting flow, such as interparticle frictional and collisional forces and those between the flow and the substrate, were considered. For a 150-m-high ridge, equation 1 yields a minimum velocity of 54 m/s or about 200 km/hr. That the debris completely overtopped the ridge without deflection and continued down the valley indicates that the velocity was significantly greater than this minimum required to reach the top of the ridge.

At 5 km from the landslide source, the valley turns 70° to the east. The avalanche debris followed this turn and flowed about 60 m up the valley walls on the outside of the turn, indicating both high velocity and fluid movement. This presents another opportunity to estimate flow velocity using a different relation given by Chow (1959) that is based on super-elevation, the elevation difference of a channelized deposit between the inside and outside of a curve (see, e.g., Evans et al. 2001, Vallance and Scott 1997, Voight and Sousa 1994):

$$v = [d(r/w)g]^{0.5}, \quad (2)$$

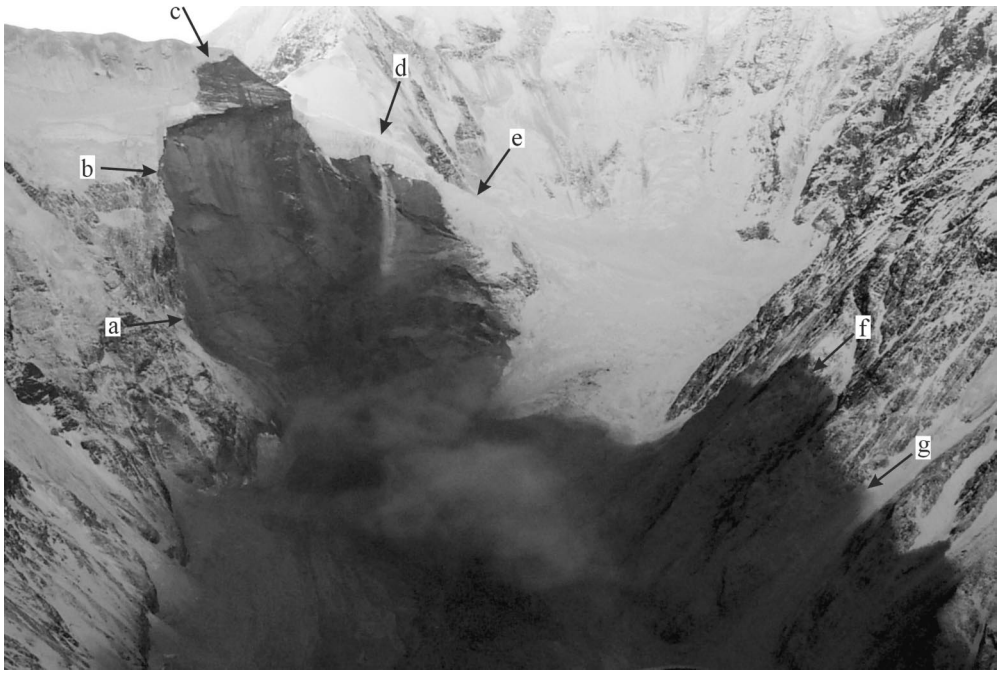

Figure 4. Source area of McGinnis Peak rock avalanche (view toward southwest). The source is defined by pre-existing discontinuities in the rock mass. The main scarp is indicated by arrows a–e. Several meters of glacial ice also failed, as visible at arrows d and e; ice is avalanching down the scar below arrow d. The dark area indicated by arrows f and g marks a line of dust that was pushed in front of the rapidly moving slide mass.

where v is velocity in meters per second, d is super-elevation in meters, r is curve radius in meters, w is channel width in meters, and g is gravitational acceleration. This equation was developed assuming that the gravitational force balances the centrifugal force that causes a flow to climb the outside wall of a curved channel. Only gravitational forces are considered to resist flow, as with equation 1; therefore, the minimum velocity is estimated. For a 60-m super-elevation, a curve radius of 3580 m, and a channel width of 1300 m, equation 2 yields a velocity of 40 m/s or about 150 km/hr. These two velocity estimates are consistent with other reported velocity estimates of seismically induced rock avalanches. Some have moved at speeds as great as 250–300 km/hr (Plafker et al. 1971).

Material exposed on the surface of the landslide deposit consists of angular rock fragments ranging from large boulders several meters on a side to fine-grained, soil-like material. The surface of the deposit also has ridges and depressions of several meters amplitude that reflect the flow characteristics of the material. The surface of the deposit is thus highly irregular and difficult to traverse.

On the inside part of the turn where the rock avalanche followed the glacier and turned to the east, possible older landslide deposits are exposed on the glacier surface.

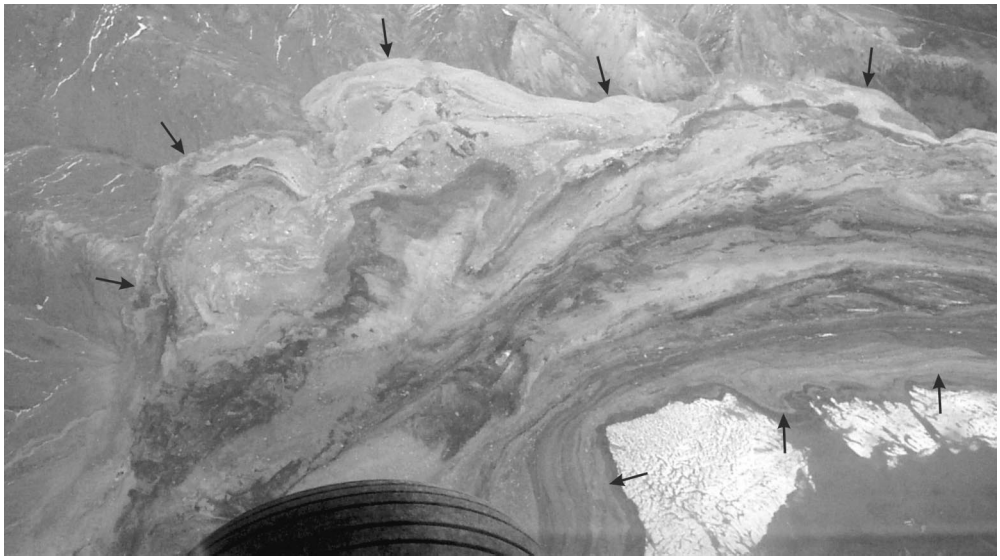

Figure 5. McGinnis Peak rock avalanche deposit (view toward north). Arrows mark edge of deposit. As the rock avalanche turned this corner, the outboard edge of the avalanche (upper center) ran about 60 m up the outside valley wall. On the inboard edge of the corner, the deposit came to rest on older rock avalanche deposits, visible in lower right corner of photo below the arrows.

The margin of the 2002 deposit is somewhat inboard (toward the inside part of the turn) of the midline of the glacier and is marked by a steep, well-defined margin 2–3 m high. This 2002 material was deposited on possible older landslide deposits that extend toward the inside of the turn (Figure 6). Our brief field inspection indicated that two, and possibly three, successively older deposits are exposed moving inward from the margin of the 2002 deposit. The morphology, texture, and lithology of the 2002 deposits are identical to those of the older deposits, suggesting similar origins. The multiple older deposits appear to differ in age from each other based on the degree of new vegetation on the surface of the deposits, the degree of weathering, and geomorphic features such as stone lines suggesting old flow boundaries.

A rock avalanche was also triggered from a source area on a ridge extending southeast from McGinnis Peak (see Figure 3). This failure involved about 8.5×10^6 m^3 of material similar to that described above. The landslide material covered virtually the entire surface of the southeastern lobe of the McGinnis Glacier, on which it traveled. The glacial surface was previously covered with rock debris, presumably from previous rock avalanches or smaller landslides from the valley margins, and the 2002 landslide covered the surface with an average depth of 1 m of new rock debris.

The two rock avalanches converged where the two lobes of the glacier converge, and both continued to travel to the snout of the glacier for a total travel distance of 11–12 km.

Figure 6. The 2002 rock-avalanche deposit has a steep, well-defined margin that extends left to right through the center of the photo (man inside circle shows scale, view toward northwest). The 2002 deposit (upper center of photo) came to rest on the material visible in the foreground, whose texture, lithology, and morphology are similar to those of the 2002 deposit, suggesting a similar origin. The material in the foreground, however, appears much older and suggests an older landslide event possibly triggered by a previous earthquake.

BLACK RAPIDS GLACIER LANDSLIDES

The earthquake triggered three large rock avalanches and several smaller ones from steep granitic slopes that form the southern edge of the valley occupied by the Black Rapids Glacier (see Figure 1). The Denali fault extends through this valley, and so the landslides occurred within a few hundred meters of the fault trace and buried the fault rupture in places. The three largest landslides had a combined volume of about 25 $\times 10^6$ m^3. They cascaded down steep rock slopes, crossed a lateral moraine at the valley's margin and a medial moraine, and then spread out about 2.5 km across the glacier-filled valley, coming to rest near the opposite valley wall (Figure 7).

Multiple joint surfaces both subparallel and orthogonal to the slope face were exposed at the landslide sources. These joint surfaces defined slabs 30–50 m thick that failed and cascaded down the 35°–38° slopes. The fractures that defined the basal failure surfaces of the two western landslides extended beneath the ridge top and emerged again on the back side of the slope; thus, the entire ridge top failed, and the main scarps define scallops in the ridge line where the previous ridge top is now missing. On the back side of the ridge, an uphill-facing scarp having about 2 m of northward displacement extends for tens of meters westward from the intersection of one of the main scarps and the new ridgeline. This fracture defines a much larger incipient failure mass that moved during the earthquake but did not catastrophically fail. This incipient failure mass with a volume of perhaps 100×10^6 m^3 could be reactivated in future earthquakes, heavy rainfall, or snowmelt episodes. The easternmost of the three landslides occurred on a ridge sepa-

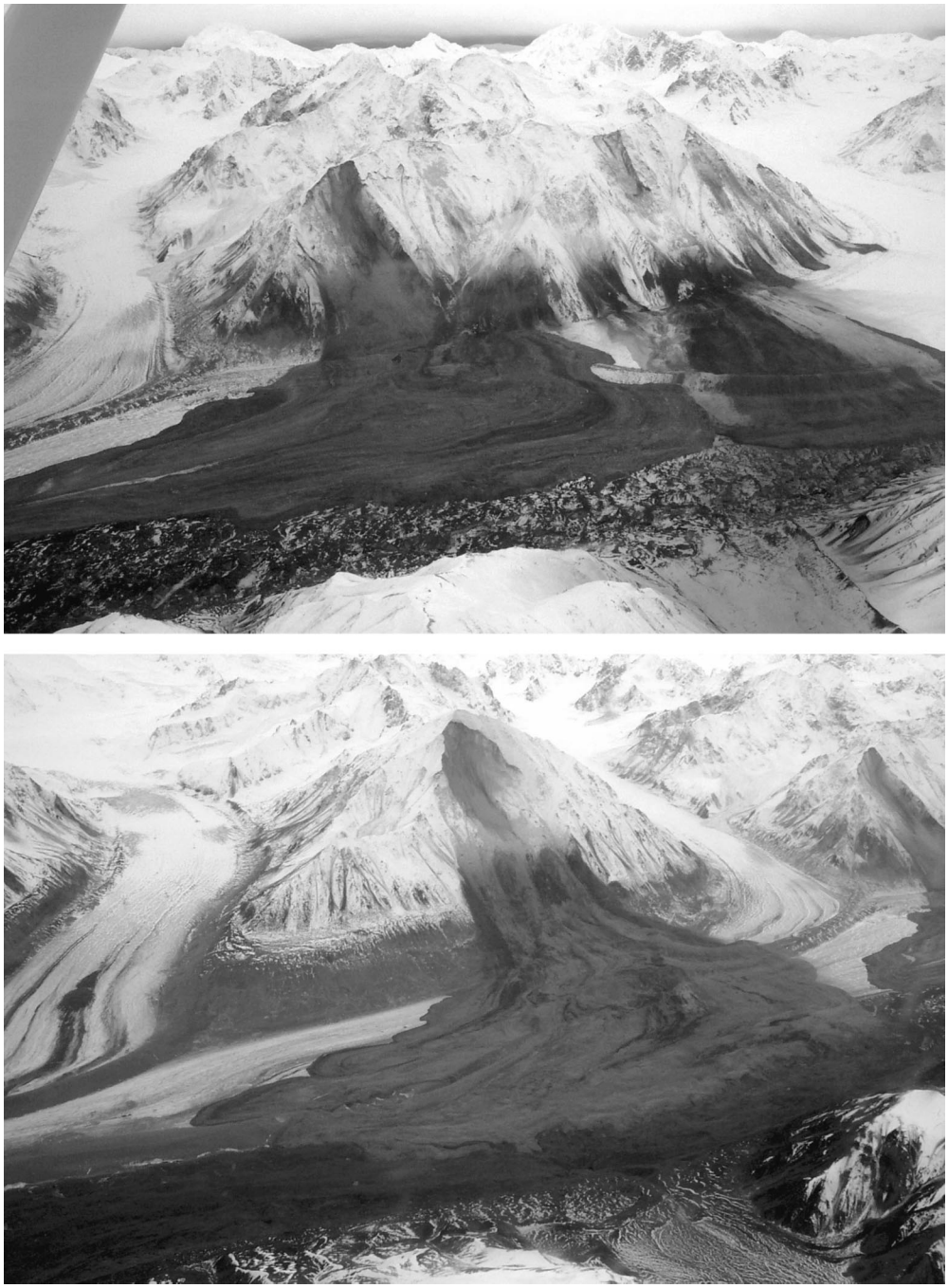

Figure 7. Black Rapids Glacier rock avalanches (views toward south). The valley glacier is about 2 km wide here. The Denali fault extends beneath the glacier near the mountain front. (a) Westernmost rock avalanches; several smaller landslides extend along the ridge to the right. (b) Eastern rock avalanche; multiple lobes of material moved semi-independently of each other.

Figure 8. Deposit of middle Black Rapids Glacier rock avalanche (view toward northwest), showing the uniform thickness and sharp edge of the deposit. Bands on surface of deposits indicate flow of different lobes of material. The glacier is about 2 km wide here.

rated by a valley glacier from the ridge on which the other two occurred. The landslide scar is similar to the other two; however, it extends to just below the mountain peak. Fractures visible in the landslide source area indicate that the entire peak forms an incipient failure that could be similarly activated.

The deposits were uniformly thin, 2–3 m in most areas, including where the avalanche debris spread up and over a 50-m-high medial moraine. Equation 1 indicates that the avalanches were moving at least 130 km/hr to cross the moraine, but they were certainly moving faster as they then traveled more than 1 km down the 1°–2° sloped glacial surface.

Two of the rock avalanches crossed the glacier and then turned and flowed some hundreds of meters down the valley on the glacier surface. From a distance, the surface of the deposits appears to have a homogeneous texture, but the surface is banded where flow features formed in the debris (Figure 8). Walking on the deposits, however, was difficult owing to the block-like debris surface. The grain-size distribution of the deposits is continuous across a broad range, from clayey and silty soil to granitic blocks several meters on a side. The margins of the deposits are sharply defined, have nearly uniform inclination of 38°, and average 2–3 m in height.

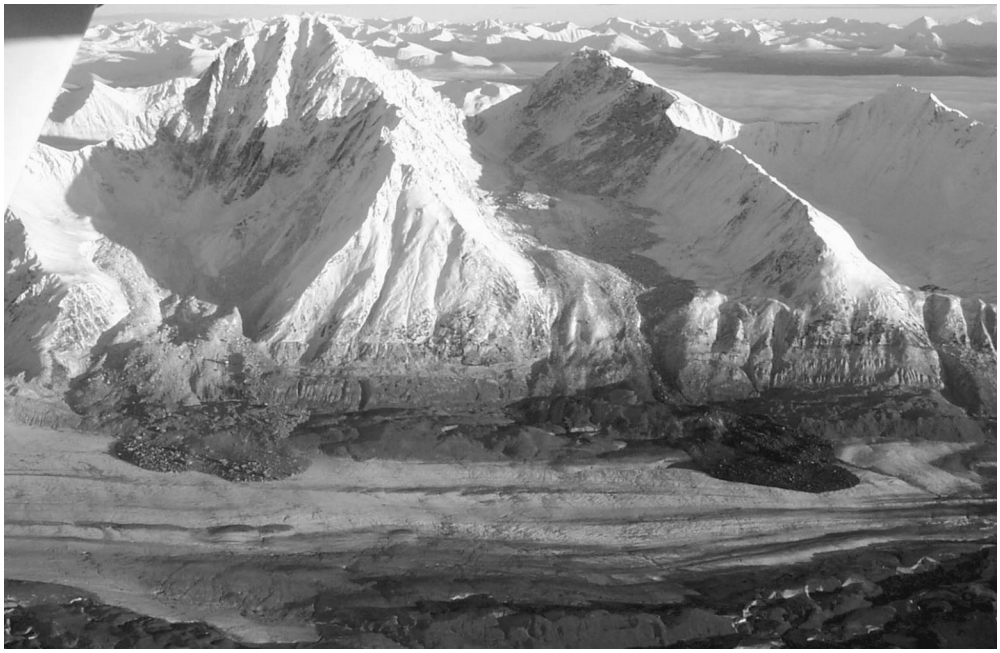

Figure 9. West Fork Glacier rock avalanches (view toward east). The surface trace of the Susitna Glacier fault lies on the far side of the mountains in the foreground. Glacier is 3–4 km wide here.

WEST FORK GLACIER LANDSLIDES

Two large rock avalanches were triggered above the West Fork Glacier (see Figure 1) from steep slopes in two adjacent glacial cirques. The dislodged rock moved rapidly down the cirques, crossed the lateral moraine at the edge of the valley, and spread out as it flowed onto the glacial surface (Figure 9). The north slide is about 2500 m long and 500–800 m wide; the south slide is about 4000 m long and 800 m wide.

Landslide material failed from multiple sources on the steep slopes of the cirques. Slopes adjacent to the source areas were deeply fissured, and large parts of these slopes only partially mobilized, leaving incipient landslide masses perched on the slopes. Large amounts of the rock-avalanche debris came to rest at the bottom of the cirques and created convex-upward deposits that covered whatever glacial ice was still there.

The lower parts of the deposits on the glacier surface consisted mainly of blocks of metamorphic rock spanning a wide range of sizes; some individual blocks measured more than 20 m on a side (Figure 10). The thickness of the deposits generally ranged between 3 and 15 m, thinner where small blocks accumulated and thicker where large blocks came to rest. The deposits had sharp, steep margins. In most places, large blocks on the leading edge of the toe appeared to have slid across the glacial ice with little gouging of the surface.

Figure 10. Large block in deposit of West Fork Glacier rock avalanche. Blocks of this size were numerous in the deposit and indicated the presence of fairly massive rock in the source area.

Each of the two rock avalanches had a volume of $2–3\times10^6$ m^3 on the glacier surface, and we estimate that landslide debris remaining in the cirques was at least twice this volume. The south rock avalanche had a significantly longer path covered with debris, thus we estimate that the total volumes of the north and south landslides were 6.5×10^6 m^3 and 11.2×10^6 m^3, respectively.

These rock avalanches showed evidence of high-speed travel. For example, one of them deposited landslide debris on a surface about 50 m above the bottom of the cirque on the wall opposite the source area. From equation 1, the velocity here was at least 113 km/hr. Also, parts of the down-hill face of the lateral moraine that was in the path of the rock avalanche were undisturbed, indicating that at least some of the avalanche debris may have been airborne and did not disturb this part of the moraine.

SACKUNGEN

Sackungen (ridge-top troughs bounded by uphill-facing scarps) formed on some ridges adjacent to the fault rupture. The two most prominent sackung locations are a ridge on the flank of the Black Rapids Glacier (about 8 km down-valley from the Black Rapids rock avalanches) and a ridge immediately west of Gillett Pass (see Figure 1). At both locations, ridge-parallel uphill-facing scarps formed on both flanks of the ridge, and graben formed on the ridge crests.

At the Black Rapids site, multiple scarps as high as 3 m formed on the ridge flanks (Figure 11). Total cumulative vertical displacement across the scarps was about 10 m.

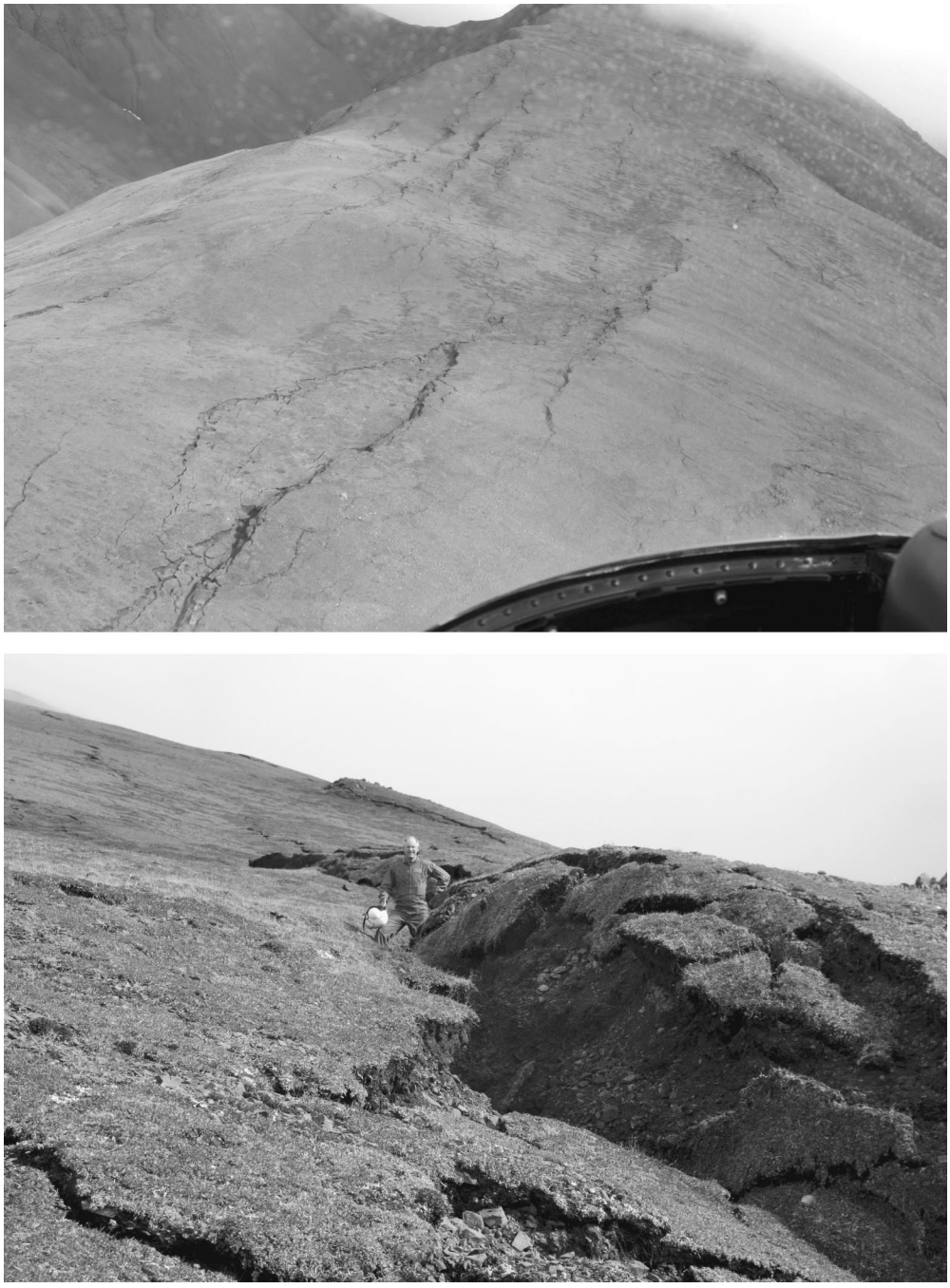

Figure 11. Sackung (see text) on ridge astride the Denali fault near the Black Rapids Glacier. (a) Multiple sets of uphill-facing scarps parallel the ridge crest for a few kilometers along the ridge. (b) Individual scarps had 1–3 m of vertical offset; cumulative vertical offset across the ridge averaged about 10 m.

Figure 12. Multiple uphill-facing scarps on ridge astride the Denali fault just west of Gillett Pass. The fractures extend between the major scarps, indicating complex internal deformation of the ridge. The fractures extend to great depth, as evidenced by their continuity through the deep ravine at the upper left.

The scarps extended about 1500 m along the ridge. Collapse of surficial soil over some fractures indicates that the fractures dilated significantly and allowed overlying soil to fall into the void. A few dilated fractures were open to depths of several meters.

Sackung features were even more extensive along a 600-m-high ridge that extends from Gillett Pass about 5 km westward. The Denali fault extends along the north flank of the ridge, and a previously unknown 6-km-long splay also ruptured along the south side of the ridge. A complex network of uphill-facing scarps extended along both ridge flanks. In addition to scarps parallel to ridge crests, scarps in several locations extended through ridges normal to the ridge crest. Some scarps had as much as 5 m of displacement, and graben formed along the ridge crest (Figure 12). Many of the scarps extended through pre-existing notches in ridges, suggesting recurrent movement. Also, older uphill-facing scarps were visible and likewise suggest earlier episodes of movement. A large debris slide formed on one ridge flank where a sackung scarp traversed a steep part of the slope. The scarp extends into the main scarp of the landslide, clearly suggesting that the formation of the sackung scarp triggered slope failure. The ridge was also extensively faulted, as evidenced by notched ridge lines at contacts of differing rock units

that are clearly in fault contact. Thus, the relative effects of shaking and tectonic deformation on the formation of the uphill-facing scarps are difficult to differentiate without more detailed investigation.

DISCUSSION

With only one seismic instrument in the near-field region, the pattern of landsliding may be one of the best indicators of the pattern of ground shaking. The Keefer (2002) relationship between area affected by landslides and earthquake magnitude shows that the mean area affected by a M7.9 earthquake is approximately 28,000 km^2, and the maximum area is about 90,000 km^2. Based on the landslide distribution shown in Figure 1, the area within which nearly all the landslides occurred in the November 3 earthquake measures only 10,000 km^2, which is roughly at the lower boundary of Keefer's (2002) data. This relatively small area affected by landslides suggests lower than average ground shaking in this earthquake. In contrast, the area affected by landslides triggered by the 1964 M9.2 Alaska earthquake was 269,000 km^2, and the farthest landslides were triggered 700 km from the epicenter (Plafker et al. 1969, Keefer 1984 and 2002).

The pattern of landsliding suggests that shaking levels necessary to trigger rock falls and rock slides generally were focused in a narrow band centered along the fault zone rather than extending radially outward for great distances. Even within this zone, the number and concentration of these slides appeared less than would be expected for an earthquake of this magnitude. Keefer (2002) indicated that earthquakes of this magnitude might be expected to trigger an average of 80,000 landslides in the epicentral area, but in the 2002 M7.9 earthquake the concentration appeared to be at least an order of magnitude less than this.

Few landslides were triggered west of the epicenter; most occurred to the east. This pattern is clearly consistent with the eastward propagation of the second and third subevents of the earthquake (Eberhart-Phillips et al. 2003, Choy and Boatwright 2004). West of the epicenter, areas of concentrated rock falls and rock slides disappear within 30 km of the epicenter, whereas to the southeast, the zone of rock falls and rock slides, concentrated in a band close to the rupture zone, extends more than 300 km along this zone.

Failures in brittle rock are most sensitive to high accelerations commonly within the higher frequencies (1–10 Hz) of ground motion. Relative to other earthquakes of comparable or lower magnitudes (the 1987 M6.9 Ecuador earthquake, the 1970 M7.1 New Guinea earthquake, the 1976 M7.0 Darien, Panama, earthquake, the 1977 M7.4 San Juan, Argentina, earthquake, and the 1970 M7.9 Peru earthquake) for which landslide concentrations have been measured or estimated (Keefer 1993), the Denali earthquake had significantly lower concentrations of rock falls and rock slides. The rupture zone along the Denali and Totschunda faults contains abundant steep slopes in highly fractured and sheared materials that should be highly susceptible to failure during seismic shaking. Thus, the relatively low concentrations of rock falls and rock slides suggests that the earthquake shaking was deficient in high-frequency, high-amplitude accelerations. Although this conclusion is tentative, the one near-field strong-motion instrument (Pump Station 10, about 3 km north of the fault rupture along the Richardson Highway,

see Figure 1) recorded a maximum horizontal acceleration of only 0.36 g, a lower peak acceleration than expected for an earthquake of this magnitude. Frankel (2004) notes, however, that this recording may not be representative of near-field ground motion because of its location midway between subevent 1, which likely produced the highest near-field accelerations, and subevent 3, which had the greatest moment release.

For comparison, the 1994 M6.7 Northridge, California, earthquake produced accelerations exceeding 1 g and triggered more than 11,000 landslides with concentrations of hundreds of slides per square kilometer (Harp and Jibson 1995 and 1996). Because the first subevent of the Denali fault earthquake was a M7.2 thrust, we would have expected to see similar landslide concentrations there as we saw from the Northridge earthquake. Although a few large rock avalanches were triggered in this area, we were surprised that the overall concentrations of landslides were significantly lower than those triggered by the Northridge earthquake, despite the fact that the Northridge earthquake was much deeper on a blind fault (Wald et al. 1996). In fact, the 2002 rock avalanches were separated by large areas of only sparse landslide activity despite the presence of abundant steep slopes in what appeared to be similarly susceptible rock.

Inversion studies by Frankel (2004) indicate that subevent 1 (the thrust event) produced by far the largest high-frequency (1–10 Hz) energy release per unit fault length. High-frequency energy moderated along the subevent-2 segment, which may explain in part the moderate ground acceleration recorded at Pump Station 10. Subevent 3, despite having the highest moment release and greatest surface slip, was relatively deficient in high-frequency energy, and the rupture of the Totschunda fault generated negligible high-frequency energy. Broadband teleseismic studies by Choy and Boatwright (2004) similarly found that accelerations generated by subevent 1 had much higher frequencies than those generated by subevents 2 and 3. Frankel et al. (2002) also showed that subevents 1 and 2 contained the highest accelerations within the available earthquake records. These conclusions are strikingly consistent with the observed landslide distribution: all of the largest landslides clustered between the first two subevents, where accelerations and high-frequency energy were highest, and landslide concentration decreased gradually eastward along the fault rupture zone.

The M7.2 thrust event that formed the first subevent probably played a major role in the triggering of the large rock avalanches, particularly those on the West Fork Glacier. These West Fork Glacier rock avalanches were on the hanging wall directly above the thrust fault, a location that has been correlated with abnormally high ground motions in past earthquakes (Abrahamson and Somerville 1996, Dalguer et al. 2001). Also, thrust earthquakes generally have higher frequency ground motion and higher accelerations than strike-slip events of similar magnitudes (Abrahamson and Silva 1997, Boore et al. 1997, and Somerville et al. 1996).

Farther to the east, the absence of large landslides near subevent 3 and along the Totschunda fault (Figure 1) suggests that shaking levels were lower there. Along this eastern part of the fault zone the topography has a somewhat softer texture—owing to the presence of more erodible sedimentary rock—than in the areas near subevents 1 and 2, but very steep slopes in weak material susceptible to slope failure are still present in this eastern zone. For example, about 15 km west of Gillett Pass, a series of very large,

ancient rock-avalanche deposits extends for several kilometers along the valley floor along the Denali fault trace. Thus, these slopes have produced rock avalanches even larger than those triggered to the west in 2002, but shaking conditions in 2002 along this part of the fault were not severe enough to trigger large landslides.

The area around the rock avalanches at Black Rapids Glacier and McGinnis Peak has high relief and many steep slopes at all orientations. All five of the large rock avalanches, however, occurred on nearly identically oriented north-northeast-facing slopes. This suggests that there may have been a large north-northeastward (that is, fault-normal) component of ground motion associated with subevents 1 or 2 or both.

Comparison of landslides and liquefaction effects casts further light on the strong-motion distribution produced by the earthquake. Whereas both liquefaction and landslides occurred within the 30-km-wide zone that straddles the fault rupture, the liquefaction effects extended significantly beyond this zone, which is unusual when compared with other earthquakes. Keefer's (1984) data from 40 worldwide earthquakes show that the epicentral distance limit for non-liquefaction-induced landslides is beyond the limit for liquefaction-induced landslides, even in the 7.5-8.5 magnitude range where the limites begin to converge. Further, the concentration of the large rock avalanches near the first two subevents is also in contrast with the broad eastward concentration of liquefaction effects in the area of the third subevent of the earthquake. In the eastern part of the area, liquefaction effects were much more extensive and deformation more severe than in areas to the west near the first and second subevents (Figure 1 and Kayen et al. 2004), despite the presence of abundant areas highly susceptible to liquefaction throughout the entire epicentral region.

We attribute the contrast in the landslide and liquefaction occurrences to the fact that landslides and liquefaction effects are sensitive to different ground-shaking parameters. Failures in brittle rock are sensitive to high accelerations commonly within the higher frequencies of ground motion. Rock failures can be triggered by very short durations of high accelerations. Liquefaction-induced failure of saturated sediment, on the other hand, is most responsive to longer-period ground shaking and depends more on the shaking duration than on short pulses of high acceleration; repetitive cycles of shear strain are required to trigger liquefaction (Seed and Lee 1966). Thus, the concentration of severe liquefaction in the eastern part of the area suggests that long-period shaking of long duration occurred there. The third subevent, near which most of the severe liquefaction occurred, produced the longest fault rupture and the greatest fault offsets, which may relate to a longer shaking duration. The second and third subevents also produced much longer-period ground motion than the first two subevents (Choy and Boatwright 2004, Frankel 2004).

The long runout distances of some of the rock avalanches merit examination. We compared the runout distances of the rock avalanches at McGinnis Peak, Black Rapids Glacier, and West Fork Glacier with those of other rock avalanches worldwide (Evans and Clague 1988; Shaller 1991). Figure 13 plots the log of landslide volume versus the ratio of length (runout) to height (total vertical drop) of 145 landslides that traveled on the ground and 38 that traveled on ice (glacial surfaces). Interestingly, most of the data cluster together regardless of substrate. The Denali Fault earthquake rock avalanches

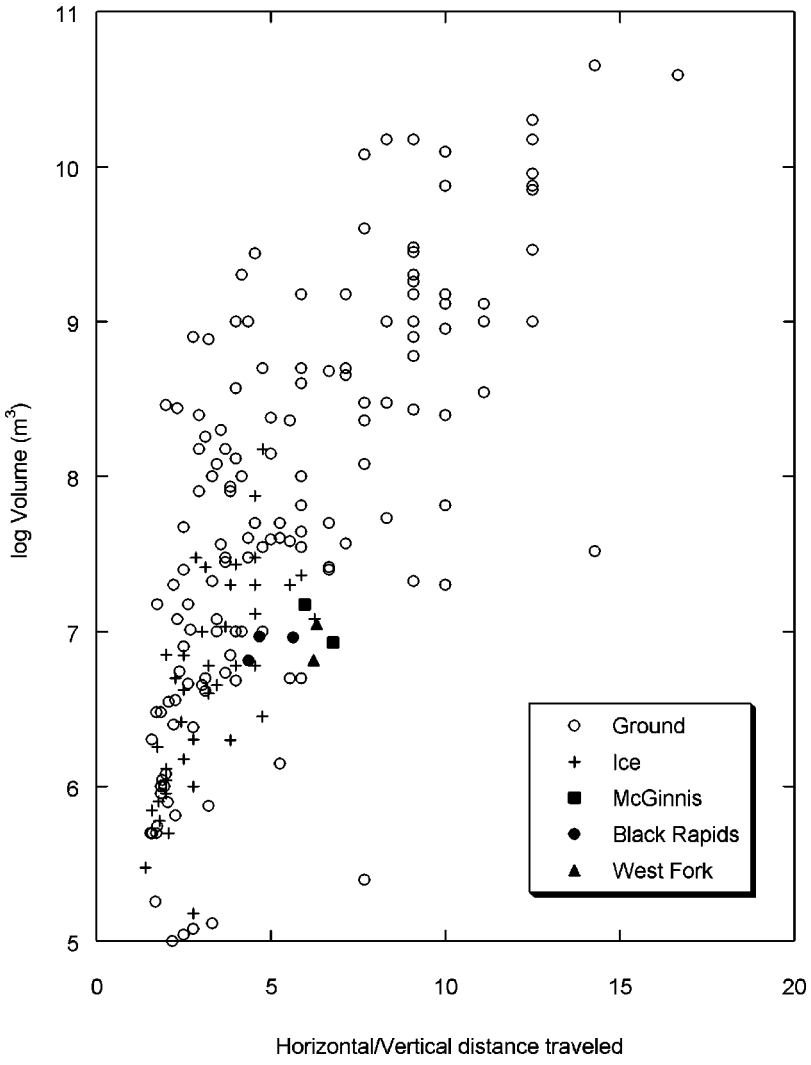

Figure 13. Plot comparing volumes of rock avalanches with the ratio of their horizontal to vertical travel distance. Rock avalanches traveling on ice (glacial surfaces) and ground generally cluster together. Rock avalanches triggered by the 2002 earthquake plot within the worldwide data, but on the long-runout side of the data. Data from Evans and Clague (1988) and Shaller (1991).

plot within the overall data cluster, but on the long-runout side of it, and plot on the long-runout edge of the data for landslides on ice. This comparison indicates that these landslides had relatively long—but not exceptional—runout distances.

The older landslide deposits exposed on the McGinnis Glacier are of particular interest because they indicate that what occurred during the 2002 earthquake could be a repeat of similar events in the past. The similarity in morphology, lithology, and texture

of these older deposits to the 2002 deposit certainly suggests a similar mechanism of deposition. If these previous landslides were also triggered by earthquake shaking, dating the older deposits could indicate the timing of earlier earthquakes. Although proving a seismic origin for these older deposits might be difficult, a seismic origin might reasonably be assumed because of the similarities in size, texture and morphology of the older and recent deposits (Jibson 1996a, b).

The well-preserved flow features and relatively uniform thickness of the deposits from the Black Rapids Glacier rock avalanches provide interesting insights into the physics of these flows. The material, despite being composed of coarse, block-like rock fragments, behaved as a viscous fluid as it flowed. A detailed analysis of this phenomenon is not included in the scope of this paper.

SUMMARY AND CONCLUSIONS

The Denali fault earthquake of 3 November 2002 triggered thousands of landslides, primarily rock falls and rock slides, that formed an unusual pattern. Unlike landslide distributions in most previous earthquakes, the triggered slides clustered in a narrow band about 30-km wide along the 300-km-long rupture zone. Several large rock avalanches, $2–15\times10^6$ m^3 in volume, were triggered, and some of these traveled as far as 12 km on the surfaces of valley glaciers. Several tentative conclusions can be drawn from the distribution of triggered landslides:

- The low concentration of landslides in the near field suggests that the earthquake was deficient in high-frequency energy and attendant high-amplitude accelerations. The single near-field recorded acceleration was only 0.36 g.
- Accelerations high enough to trigger landslides extended relatively short distances, only about 15 km, from the zone of fault rupture.
- The clustering of large rock avalanches within the areas of the first two subevents of the earthquake is consistent with these subevents containing the highest accelerations and greatest amount of high-frequency energy in the earthquake record. No large rock avalanches were present in the area of the third subevent, which generated large fault displacements but relatively lower accelerations and less high-frequency energy.
- Landslides extended only short distances to the west of the epicentral area of the earthquake whereas to the east they extended for more than 300 km along the zone of fault rupture, presumably because of the eastward directivity of shaking that attended the eastward propagation of fault rupture.
- Liquefaction features were primarily concentrated in the eastern part of the rupture zone, well beyond the zone of concentrated landslides. This could have been a consequence of the longer duration of shaking in the third subevent.
- The presence of older rock-avalanche deposits that are similar to the 2002 deposits indicates that the 2002 event was a repeat of earlier, similar events. Dating these deposits could provide insight into the timing of earlier earthquakes.

Soon after the earthquake, we suggested that the distribution of triggered ground failures (landslides and liquefaction) could tell us something about the characteristics of

the near-field ground motions (Eberhart-Phillips et al. 2003; Harp et al. 2003). The consistency of these early hypotheses with the results of later seismological studies (Choy and Boatwright 2004, Frankel 2004), as discussed in detail in this paper, demonstrates the usefulness of detailed characterization and analysis of post-earthquake ground-failure distributions. Certainly in areas where near-field strong-motion instruments are absent or sparse, analysis of the distribution of shaking-induced ground failures can play a key role in interpreting—even if only with a broad brush—the near-field ground motions.

REFERENCES

Abrahamson, N. A., and Silva, W. J., 1997. Empirical response spectral attenuation relations for shallow crustal earthquakes, *Seismol. Res. Lett.* **68**, 94–127.

Abrahamson, N. A., and Somerville, P., 1996. Effects of the hanging wall and footwall on ground motions recorded during the Northridge earthquake, *Bull. Seismol. Soc. Am.* **86** (1B), S93–S99.

Boore, D. M., Joyner, W. B., and Fumal, T. E., 1997. Equations for estimating horizontal response spectra and peak acceleration from western North American earthquakes: A summary of recent work, *Seismol. Res. Lett.* **68**, 128–153.

Chow, V. T., 1959. *Open-channel hydraulics*, McGraw-Hill, New York, p. 680.

Choy, G. L., and Boatwright, J., 2004. Radiated energy and the rupture process of the Denali Fault earthquake of 2002 from broadband teleseismic body waves, *Bull. Seismol. Soc. Am.* in press.

Dalguer, L. A., Irikura, K., Riera, J. D., and Chiu, H. C., 2001. The importance of the dynamic source effects on strong ground motion during the Chi-Chi, Taiwan, earthquake: Brief interpretation of the damage distribution on buildings, *Bull. Seismol. Soc. Am.* **91**, 1112–1127.

Eberhart-Phillips, D., Haeussler, P. J., Freymueller, J. T., Frankel, A. D., Rubin, C. M., Craw, P., Ratchkovski, N. A., Anderson, G., Carver, G. A., Crone, A. J., Dawson, T. E., Fletcher, H., Hansen, R., Harp, E. L., Harris, R. A., Hill, D. P., Hreinsdóttir, S., Jibson, R. W., Jones, L. M., Kayen, R., Keefer, D. K., Larsen, C. F., Moran, S. C., Personius, S. F., Plafker, G., Sherrod, B., Sieh, K., Sitar, N., and Wallace, W. K., 2003. The 2002 Denali fault earthquake, Alaska: A large magnitude, slip-partitioned event, *Science* **300**, 1113–1118.

Evans, S. G., and Clague, J. J., 1988. Catastrophic rock avalanches in glacial environments, in Bonnard, C., ed., *Proceedings, 5th International Symposium on Landslides*, Lausanne, Switzerland, **2**, 1153–1159.

Evans, S. G., Hungr, O., and Clague, J. J., 2001. Dynamics of the 1984 rock avalanche and associated distal debris flow on Mount Cayley, British Columbia, Canada; implications for landslide hazard assessment on dissected volcanoes, *Eng. Geol. (Amsterdam)* **61**, 29–51.

Frankel, A. D., 2004. Rupture process of the M7.9 Denali fault, Alaska, earthquake: Subevents, directivity, and scaling of high-frequency ground motions, *Bull. Seismol. Soc. Am.* in press.

Frankel, A. D., Biswas, N. N., Martirosyan, A. H., Dutt, U., and McNamara, D. E., 2002. Rupture process of the M7.9 Denali fault, Alaska, earthquake determined from strong-motion recordings, *EOS Trans. Am. Geophys. Union* **47**, 1340.

Harp, E. L., and Jibson, R. W., 1995. Inventory of landslides triggered by the 1994 Northridge, California, earthquake, *Open-File Rep. 95–213, U. S. Geol. Surv.*, 17 pp.

Harp, E. L., and Jibson, R. W., 1996. Landslides triggered by the 1994 Northridge, California, earthquake, *Bull. Seismol. Soc. Am.* **86** (1B), S319–S332.

Harp, E. L., Jibson, R. W., Kayen, R. E., Keefer, D. K., Sherrod, B. L., Carver, G. A., Collins, B. D., Moss, R. E. S., and Sitar, N., 2003. Landslides and liquefaction triggered by the M7.9 Denali fault earthquake of 3 November 2002, *GSA Today* **13** (8), 4–10.

Jibson, R. W., 1996a. Use of landslides for paleoseismic analysis, *Eng. Geol. (Amsterdam)* **43**, 291–323.

Jibson, R. W., 1996b. Using landslides for paleoseismic analysis, chapter 8 in McCalpin, J. P. (ed.), *Paleoseismology*, Academic Press, Inc., San Diego, pp. 397–438.

Kayen, R. E., Thompson, E., Minasian, D., Collins, B. D., Moss, R. E. S., Sitar, N., and Carver, G. A., 2004. Geotechnical reconnaissance of the 2002 M7.9 Denali Fault earthquake, *Earthquake Spectra* **20** (3), 639–667 (this issue).

Keefer, D. K., 1984. Landslides caused by earthquakes, *Bull. Geol. Soc. Am.* **95**, 406–421.

Keefer, D. K., 1993. The susceptibility of rock slopes to earthquake-induced failure, *Bull. Int. Assoc. Eng. Geol.* **30**, 353–361.

Keefer, D. K., 2002. Investigating landslides caused by earthquakes—an historical review, *Surveys in Geophysics* **23**, 473–510.

Kikuchi, M., and Yamanaka, Y., 2002. Source rupture processes of the central Alaska earthquake of Nov. 3, 2002, inferred from teleseismic body waves (the 10/23 M6.7 event), *EIC Seismol. Note*, no. 129.

Miller, M. L., Bradley, D. C., Bundtzen, T. K., and McClelland, W., 2002. Late Cretaceous through Cenozoic strike-slip tectonics of southwestern Alaska, *J. Geol.* **110**, 247–270.

Plafker, G., Ericksen, G. E., and Fernández, C. J., 1971. Geological aspects of the May 31, 1970, Peru earthquake, *Bull. Seismol. Soc. Am.* **61**, 543–578.

Plafker, G., Gilpin, L. M., and Lahr, J. C., 1994. Neotectonic map of Alaska, in Plafker, G., and Berg, H. C. (eds.), *The Geology of Alaska*, Geological Society of America, Boulder, CO, plate 12.

Plafker, G., Hudson, T., and Richter, D. H., 1977. Preliminary observations on late Cenozoic displacements along the Totschunda and Denali fault systems, *U. S. Geol. Surv. Circular 751-B*, pp. B67–B69.

Plafker, G., Kachadoorian, R., Eckel, E. B., and Mayo, L. R., 1969. Effects of the earthquake of March 27, 1964 on various communities, *U. S. Geol. Surv. Professional Paper 542-G*, 50 pp.

Post, A., 1967. Effects of the March 1964 Alaska earthquake on glaciers, *U. S. Geol. Surv. Professional Paper 554-D*, 42 pp.

Seed, H. B., and Lee, K. L., 1966. Liquefaction of saturated sands during cyclic loading, *J. Struct. Div. ASCE* **92** (SM6), 105–134.

Shaller, P. J., 1991. *Analysis and implications of large Martian and terrestrial landslides*, Ph.D. Dissertation, California Institute of Technology, p. 586.

Somerville, P., Saikia, C., Wald, D., and Graves, R., 1996. Implications of the Northridge earthquake for strong ground motions from thrust faults, *Bull. Seismol. Soc. Am.* **86** (1B), S115–S125.

Tuthill, S. J., and Laird, W. M., 1966. Geomorphic effects of the earthquake of March 27, 1964, in the Martin-Bering Rivers area, Alaska, *U. S. Geol. Surv. Professional Paper 543-B*, pp. 1–29.

Vallance, J. W., and Scott, K. M., 1997. The Osceola mudflow from Mount Rainier: sedimentology and hazard implications of a huge clay-rich debris flow, *Bull. Geol. Soc. Am.* **109**, 143–163.

Varnes, D. J., 1978. Slope movement types and processes, in Schuster, R. L., and Krizek, R. J.

(eds.), *Landslides—Analysis and Control*, Transportation Research Board, National Academy of Science, Special Report 176, pp. 11–33.

Voight, B., and Sousa, J., 1994. Lessons from Ontake-san: A comparative analysis of debris avalanche dynamics, *Eng. Geol. (Amsterdam)* **38**, 261–297.

Wald, D. J., Heaton, T. H., and Hudnut, K. W., 1996. The slip history of the 1994 Northridge, California, earthquake determined from strong-motion, teleseismic, GPS, and leveling data, *Bull. Seismol. Soc. Am.* **86** (1B), S49–S70.

(Received 1 December 2003; accepted 18 February 2004)